Identifying roles for peptidergic signaling in mice

Kathryn G. Powers[a], Xin-Ming Ma[a], Betty A. Eipper[a,b], and Richard E. Mains[a,1]

[a]Department of Neuroscience, University of Connecticut Health Center, Farmington, CT 06030-3401; and [b]Department of Molecular Biology and Biophysics, University of Connecticut Health Center, Farmington, CT 06030-3401

Edited by Tomas Hökfelt, Karolinska Institutet, Stockholm, Sweden, and approved August 1, 2019 (received for review June 18, 2019)

Despite accumulating evidence demonstrating the essential roles played by neuropeptides, it has proven challenging to use this information to develop therapeutic strategies. Peptidergic signaling can involve juxtacrine, paracrine, endocrine, and neuronal signaling, making it difficult to define physiologically important pathways. One of the final steps in the biosynthesis of many neuropeptides requires a single enzyme, peptidylglycine α-amidating monooxygenase (PAM), and lack of amidation renders most of these peptides biologically inert. PAM, an ancient integral membrane enzyme that traverses the biosynthetic and endocytic pathways, also affects cytoskeletal organization and gene expression. While mice, zebrafish, and flies lacking *Pam* ($Pam^{KO/KO}$) are not viable, we reasoned that cell type-specific elimination of *Pam* expression would generate mice that could be screened for physiologically important and tissue-specific deficits. Conditional $Pam^{cKO/cKO}$ mice, with loxP sites flanking the 2 exons deleted in the global $Pam^{KO/KO}$ mouse, were indistinguishable from wild-type mice. Eliminating *Pam* expression in excitatory forebrain neurons reduced anxiety-like behavior, increased locomotor responsiveness to cocaine, and improved thermoregulation in the cold. A number of amidated peptides play essential roles in each of these behaviors. Although atrial natriuretic peptide (ANP) is not amidated, *Pam* expression in the atrium exceeds levels in any other tissue. Eliminating *Pam* expression in cardiomyocytes increased anxiety-like behavior and improved thermoregulation. Atrial and serum levels of ANP fell sharply in PAM myosin heavy chain 6 conditional knockout mice, and RNA sequencing analysis identified changes in gene expression in pathways related to cardiac function. Use of this screening platform should facilitate the development of therapeutic approaches targeted to peptidergic pathways.

amidation | atrium | excitatory neurons | RNAseq | clock genes

Peptidergic signaling plays a key role in the vertebrate nervous system and in the simplest animals, *Trichoplax adhaerens* (tiny disk-shaped creatures), in which 6 distinct cell types do not include neurons or muscles (1, 2). Transcripts encoding putative *T. adhaerens* prepronеuropeptides are expressed in a cell type-specific manner, and amidated peptides that could be derived from them govern movement and contractile behavior (2). Acting as cotransmitters and neuromodulators in organisms with a nervous system, neuropeptides play critical roles in the complex pathways that control pain perception, mating behaviors, anxiety, appetite, and metabolism (3).

Bioactive neuropeptide synthesis in *Trichoplax* and mammals likely involves a similar set of posttranslational modifications, each of which occurs in the lumen of the secretory pathway (4–7). The bioactive peptides are stored in secretory granules and released in response to an appropriate stimulus. The vast majority of neuropeptides act through G protein-coupled receptors (GPCRs), which may be located close to or far from the site at which the bioactive peptide is released (8). Neuropeptides were identified using bioassays, biochemical paradigms, screens for GPCR ligands, and genetic selections. Some bioactive peptides, such as neuropeptide Y (NPY), were identified by the presence of a common posttranslational modification, C-terminal amidation, which is often essential for bioactivity (8, 9).

Prepronеuropeptides that yield amidated products encode precursors that generate a peptidylglycine intermediate. Peptidylglycine α-amidating monooxygenase (PAM; Enzyme Commission 1.4.17.3) catalyzes the 2-step conversion of the penultimate residue of its peptidylglycine substrate into an α-amide, releasing glyoxylate (8). Cell culture experiments have revealed additional noncanonical roles for PAM in regulating cytoskeletal organization, secretagogue responsiveness, and gene expression (10). PAM knockout mice ($Pam^{KO/KO}$), zebrafish, and *Drosophila* are not viable (11–13). $Pam^{KO/KO}$ mouse embryos develop pericardial edema, have a poorly developed yolk sac vasculature, and do not survive beyond the second week of gestation (11). Mice with a single copy of *Pam* are sensitive to seizures, exhibit increased anxiety-like behavior, and cannot maintain body temperature in the cold (14). Genetic studies indicate that *PAM* is associated with diabetes, Alzheimer disease, Parkinson disease, hypertension, and pituitary tumors (reviewed in ref. 8).

We hypothesized that generation of a mouse line in which *Pam* expression can be eliminated in a cell type-specific manner would facilitate the identification of behaviors and metabolic pathways in which neuropeptides and PAM play significant roles. LoxP sites were placed around the exons eliminated in the $Pam^{KO/KO}$ mouse (11), generating the conditional $Pam^{cKO/cKO}$ mouse. Knowing that behaviors rely on precisely balanced inputs from excitatory and inhibitory neurons, both of which express PAM (15), we bred $Pam^{cKO/cKO}$ mice to mice expressing Cre recombinase in their forebrain excitatory neurons under control of the empty spiracles homeobox 1 promoter (Emx1-Cre) (16, 17); excitatory neurons account for at least 75% of the neurons in the central nervous system. Given the high levels of PAM expressed in atrial cardiomyocytes (18), we also bred $Pam^{cKO/cKO}$

Significance

Peptidergic signaling, which plays key roles in the many pathways that control thermoregulation, salt and water balance, metabolism, anxiety, pain perception, and sexual reproduction, is essential for the maintenance of homeostasis. Despite the fact that peptides generally signal through G protein-coupled receptors, it has proven difficult to use knowledge about peptide synthesis, storage, and secretion to develop effective therapeutics. Our goal was to develop an in vivo bioassay system that would reveal physiologically meaningful deficits associated with disturbed peptidergic signaling. We did so by developing a system in which an enzyme essential for the production of many bioactive peptides could be eliminated in a tissue-specific manner.

Author contributions: B.A.E. and R.E.M. designed research; K.G.P., X.-M.M., B.A.E., and R.E.M. performed research; B.A.E. and R.E.M. contributed new reagents/analytic tools; K.G.P., X.-M.M., B.A.E., and R.E.M. analyzed data; and K.G.P., B.A.E., and R.E.M. wrote the paper.

The authors declare no conflict of interest.

This article is a PNAS Direct Submission.

Data deposition: The data reported in this paper have been deposited in the Gene Expression Omnibus (GEO) database, https://www.ncbi.nlm.nih.gov/geo (accession no. GSE132180).

See Commentary on page 19774.

[1]To whom correspondence may be addressed. Email: mains@uchc.edu.

This article contains supporting information online at www.pnas.org/lookup/suppl/doi:10.1073/pnas.1910495116/-/DCSupplemental.

First published August 27, 2019.

mice to mice expressing Cre recombinase under control of the cardiac myosin heavy chain 6 promoter (Myh6-Cre) (19, 20). Tests of anxiety-like behavior and thermal regulation demonstrated alterations in both lines. Although atrial natriuretic peptide (ANP) is not amidated, ANP levels fell dramatically in $Pam^{Myh6\text{-}cKO/cKO}$ mice, and gene expression was altered, raising the possibility that loss of PAM protein, not PAM activity, was critical.

Using the $Pam^{cKO/cKO}$ mouse, PAM expression and amidated peptide levels can be altered in selected cell types when developmentally or experimentally expedient. In this way, it should be possible to identify the circuits and complex peptidergic pathways that play key roles in behaviors of interest.

Methods

All work with mice was approved by the University of Connecticut Health Center Institutional Animal Care and Use Committee.

Biochemical Analyses. Lysates for peptidylglycine alpha-amidating monooxygenase (PHM) and peptidyl-hydroxyglycine alpha-amidating lyase (PAL) assays were prepared by homogenizing tissue in 20 mM Na TES (N-tris[Hydroxymethyl]methyl-2-amino ethanesulfonic acid, 10 mM mannitol, and 1% TX-100, pH 7.4 with protease inhibitors; all manipulations were carried out on ice as described (21). Lysates for sodium dodecyl sulfate polyacrylamide gel electrophoresis (SDS/PAGE) were prepared using SDS-P buffer with protease inhibitor mixture (50 mM Tris, 1% SDS, 130 mM NaCl, 10 mM Na pyrophosphate, 50 mM NaF, 5 mM ethylenediamine tetracetic acid, pH 7.6); after boiling and sonication, particulate material was removed (22). Lysates were also prepared by sonication into ice-cold RIPA Buffer (#9806; Cell Signaling Technologies) containing protease inhibitors (Sigma P8340; MilliporeSigma); particulate material was then removed. Protein concentrations were determined using the bicinchoninic acid assay (Thermo Fisher), with bovine serum albumin as the standard. For PHM and PAL activity assays, samples were diluted to 0.1 mg/mL and assayed in triplicate. Amounts and assay times were adjusted to ensure assay linearity: atrium (0.2 μg, 30 min), ventricle (1.0 μg, 120 min), cortex (5.0 μg, 60 min), hypothalamus (2.0 μg, 60 min), and olfactory bulb (1.0 μg, 60 min).

For western blots, samples were denatured in SDS sample buffer by heating at 95 °C for 5 min: for atrium, 5 or 10 μg of protein was loaded; for all other tissues, 10 or 20 μg of protein was loaded (21). Samples fractionated on Bio-Rad Criterion TGX Precast 4 to 15% gradient gels were transferred to Immobilon-P transfer membranes (Millipore). Membranes were blocked with 5% milk in Tween-20 Tris-buffered saline before overnight incubation with primary antibody and visualization using horseradish peroxidase-tagged secondary antibody (Jackson ImmunoResearch Laboratories) and SuperSignal West Pico PLUS Chemiluminescent substrate (ThermoFisher). Proatrial natriuretic peptide (proANP) was detected using rabbit polyclonal antibody to proANP(1–16) (provided by Christopher Glembotski, San Diego State University, San Diego, CA) (23, 24); ANP was detected with a goat antibody (ab190001; Abcam). PAM was visualized using affinity-purified rabbit polyclonal antibodies to the linker region separating PHM from PAL in PAM-1 (JH629; RRID:AB_2721274) (21) and to the extreme cytoplasmic domain of PAM (C-Stop: RRID:AB_2801640) (25). In addition to using Coomassie Brilliant Blue staining to verify equal loading, IQ motif containing GTPase activating protein (Iqgap) was visualized using a mouse monoclonal antibody (#610611; BD Transduction Laboratories). Western blot signals in the linear range were densensitized using GeneTools software (Syngene).

The enzyme-linked immunosorbent assay (ELISA) for ANP was performed as described (EIAM-ANP-1; RayBiotech) except that the standard curve was modified to include 4-fold dilutions from 80 to 0.0195 pg; values were calculated using a logit-log transformation. Tissue and serum samples were prepared as described by de Bold and coworkers (26) and Smithies and coworkers (27) using UltraMicroSpin C18 silica columns (Nest Group). Serum renin levels were determined using an ELISA kit (ELM-Renin1-1; RayBiotech).

Tissue and Cellular Specificity of PAM Ablation. As an initial determination of the sites of PAM depletion, Myh6-Cre and Emx1-Cre mice were individually crossed with TdTomato reporter mice, and $Pam^{Emx1\text{-}cKO/cKO}$ mice were studied directly (28). Direct observation of PAM at the cellular level was accomplished by immunocytochemistry as described (29) using affinity-purified PAM polyclonal antibody JH629. Nuclei were visualized with Hoechst stain, and where indicated, glutamic acid decarboxylase 67 (GAD67) was visualized using a mouse monoclonal antibody (clone 1G10.2; Millipore) (30). Confocal imaging was performed on 12-μm sections with a Zeiss LSM 880 microscope with a 20×, 40×, or 63× objective; where indicated, *z* stacks were taken, and a single image is shown.

Behavioral and Physiological Analyses. All experiments were performed in the same circadian period (0900 to 1600 hours). Mice were handled by the same animal tester for 60 s a day for 2 d before determining the fraction of time in the open area of the elevated 0 maze (San Diego Instruments) (31). Mice were video recorded once for 5 min; times were obtained by watching the movies. Next, the general mobility and motor coordination of the mice were tested using the open field and rotarod (28, 31). Rotarod testing was performed 3 times a day for 3 d using a Five Lane Rota-Rod for Mouse (Med Associates). Each trial lasted no longer than 5 min, with the speed increasing from 4 to 40 rpm. The longest time recorded for each day was used in the analysis. Open field ambulations were recorded for 15 to 45 min (in the figures) in a Photobeam Activity System Open Field (San Diego Instruments). When the locomotor response to cocaine was tested, cocaine was administered by intraperitoneal (i.p.) injection, and open field ambulations were recorded for 45 min on successive days or after a brief withdrawal period; cocaine injections were 10 mg/kg except for day 2, which was 20 mg/kg (32, 33).

Core body temperature was recorded over a 3-h period using a rectal thermometer (14). Temperature readings were collected before entering the 4 °C cold room and once each following hour in the cold room. During the 3-h experiment, mice were singly housed in plain prechilled mouse cages with no bedding, food, or water. Abdominal and tail temperatures during 20-min restraint in an unfamiliar environment (ventilated 50-mL tube) at room temperature were determined using a Hti Dual Laser Infrared Thermometer (34, 35). Blood pressure was determined using the tail cuff method (CODA Multi Channel, Computerized, Non-Invasive Blood Pressure System for Mice and Rats; Kent Scientific Corporation) (27, 36, 37); arterial blood pressures by tail cuff method or telemetry are identical with experienced operators (36). Dietary NaCl was varied using standard mouse chows from Envigo: diet TD.96208 contained 0.49% NaCl; the high-salt diet TD.92012 contained 8% NaCl. The standard chow in the University of Connecticut Health Center Animal Tower was the irradiated version of the Teklad Global 18% Rodent Diet (2918) from Envigo and contained 0.49% NaCl, which we refer to as a normal salt diet. The effect of elimination of sympathetic nervous system input on systemic blood pressure was determined 10 min after intraperitoneal (i.p.) injection of 0.9% saline (control) or hexamethonium (30 mg/kg; # 4111; Tocris) in saline (37, 38).

For behavioral testing, control animals (CON) included wild-type (WT) mice and mice with 1 or 2 floxed *Pam* alleles but no Cre recombinase or Cre recombinase but no floxed *Pam* alleles, since these mice were behaviorally and biochemically indistinguishable from WT mice. Only WT mice were used as controls in physiological testing (e.g., blood pressure). Since males and females did not differ within a genotype except for body weight and blood pressure values, data were pooled across sexes for each genotype.

Data and Unique Materials Availability. All data are presented in the text and *SI Appendix*. All protocols are described in *Methods* or the *SI Appendix*. Sequencing data are available at GEO (GSE132180). The PAM^{cKO} mice will be available from The Jackson Laboratory as JAX#034076.

Statistical Analyses. Student *t* tests were applied in pairwise comparisons of enzyme activity or protein abundance (Excel or OpenOffice). Time courses (e.g., growth curves, ambulations after cocaine injection) were subjected to 2-way ANOVA (Prism 8). RNA sequencing (RNAseq) differential expression was evaluated using differential expression RNA sequencing 2 (DESeq2), which has its own built-in statistical comparisons.

Details of the creation of the conditional mice, genotyping, and breeding are in *SI Appendix* as are details of RNA sequencing.

Results

Mice Lacking *Pam* Expression Driven by Emx1-Cre or Myh6-Cre Grow and Perform Locomotor Tasks Normally. PAM activity is detected in mouse embryos by embryonic day 12.5 (E12.5); embryos unable to express *Pam* are not found after E14.5 (11). Since Emx1-Cre is active by E10.5 (16) and an Myh6-LacZ reporter is expressed in the E9.5 atrium (20), it is likely that Cre recombinase-mediated excision of *Pam* exons 2 and 3 occurs before expression of *Pam* would have begun. In the tissues and sera of adult heterozygous global *Pam* knockout mice ($Pam^{KO/+}$), PAM activity and protein levels are approximately half of WT values (11).

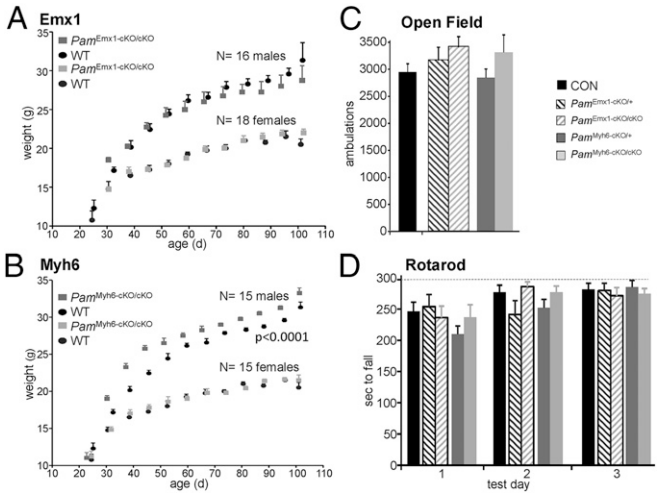

Fig. 1. Mice from both Cre-driver lines grow and move normally. Growth curves. (*A*) The growth of male ($n = 15$) and female ($n = 16$) $Pam^{Emx1\text{-}cKO/cKO}$ mice was indistinguishable from WT littermates. (*B*) $Pam^{Myh6\text{-}cKO/cKO}$ males were larger than WT male littermates ($n = 16$), while the corresponding females were indistinguishable from WT females ($n = 18$). (*C*) Open field locomotor activity. Ambulations (beam breaks) were recorded over a 30-min period: CON, $n = 43$; $Pam^{Emx1\text{-}cKO/+}$, $n = 22$; $Pam^{Emx1\text{-}cKO/cKO}$, $n = 24$; $Pam^{Myh6\text{-}cKO/+}$, $n = 26$; and $Pam^{Myh6\text{-}cKO/cKO}$, $n = 19$. For *C* and *D*, males and females were pooled, since they were indistinguishable. (*D*) Rotarod. Longest time to fall from the accelerating rotarod on each test day is plotted: CON, $n = 22$; $Pam^{Emx1\text{-}cKO/+}$, $n = 8$; $Pam^{Emx1\text{-}cKO/cKO}$, $n = 16$; $Pam^{Myh6\text{-}cKO/+}$, $n = 16$; and $Pam^{Myh6\text{-}cKO/cKO}$, $n = 8$.

For both tissue-specific $Pam^{cKO/cKO}$ lines, females grew normally from weaning to 100 d of age (Fig. 1 *A* and *B*); $Pam^{Emx1\text{-}cKO/cKO}$ male mice did not differ from WT males, while $Pam^{Myh6\text{-}cKO/cKO}$ males were slightly larger than WT ($P < 0.0001$, 2-way ANOVA). When $Pam^{Emx1\text{-}cKO/+}$ mice were mated with $Pam^{cKO/+}$ mice, the genotypes of progeny tested at weaning occurred in the expected Mendelian ratio ($n = 226$; not significant [N.S.] by 2-way ANOVA) (*SI Appendix*, Fig. S2*A*). Similarly, when Myh6-Cre progeny were tested, the expected Mendelian ratio of genotypes was observed ($n = 198$; N.S. by 2-way ANOVA) (*SI Appendix*, Fig. S2*B*).

Since most behavioral tests require normal mobility, we tested male and female $Pam^{Emx1\text{-}cKO/cKO}$ and $Pam^{Myh6\text{-}cKO/cKO}$ mice on the rotarod and in the open field. Since no differences were observed in the behavior of WT, $Pam^{cKO/cKO}$, $Pam^{cKO/+}$, and Emx1-Cre or Myh6-Cre mice, all were used as CON. The $Pam^{Emx1\text{-}cKO/cKO}$ and $Pam^{Myh6\text{-}cKO/cKO}$ mice were as active as control mice in the open field (Fig. 1*C*); no differences were observed in the performance of male and female mice. Male and female $Pam^{Emx1\text{-}cKO/cKO}$ and $Pam^{Myh6\text{-}cKO/cKO}$ mice performed as well as control mice on the rotarod (Fig. 1*D*); no differences were observed between male and female mice.

***Pam* Knockout Is Tissue Specific and Effective.** We used assays for PHM and PAL enzyme activity to assess the success of our knockout strategies. In order to extract both soluble and membrane forms of PAM, tissue from adult male and female mice was homogenized in lysis buffer containing 1% TX-100; similar results were obtained using both assays (Fig. 2 *A* and *B*). PHM- and PAL-specific activities were reduced to 25% of WT values in cortical and olfactory bulb lysates prepared from $Pam^{Emx1\text{-}cKO/cKO}$ mice. A less extreme reduction in PHM- and PAL-specific activities was also observed in hypothalamic lysates prepared from $Pam^{Emx1\text{-}cKO/cKO}$ mice. PHM- and PAL-specific activities were reduced to 2% of WT values in the atria of $Pam^{Myh6\text{-}cKO/cKO}$ mice. PHM- and PAL-specific activities, which are much lower in the adult ventricle, were reduced to 25% of WT values in $Pam^{Myh6\text{-}cKO/cKO}$ mice. In contrast, the specific activities of both enzymes in the atria and ventricles of $Pam^{Emx1\text{-}cKO/cKO}$ mice were equal to WT values, and PHM- and PAL-specific activities in lysates prepared from the sensory motor cortices of $Pam^{Myh6\text{-}cKO/cKO}$ mice did not differ from WT values.

Finally, western blot analyses of lysates prepared from $Pam^{Emx1\text{-}cKO/cKO}$ and $Pam^{Myh6\text{-}cKO/cKO}$ mice confirmed the enzyme assay results. In the atrium, intact PAM (110 kDa) was the major product, with smaller amounts of soluble PHM (40 kDa) (Fig. 2 *C* and *E*). In both cortex and hypothalamus, soluble PHM was the major product, and levels were unaltered in $Pam^{Myh6\text{-}cKO/cKO}$ mice. In contrast, in the cortex and hypothalamus of $Pam^{Emx1\text{-}cKO/cKO}$ mice, levels of both intact PAM and soluble PHM were reduced compared with WT levels (Fig. 2 *D* and *E*). PAM protein levels were unaltered in the atria and ventricles of $Pam^{Emx1\text{-}cKO/cKO}$ mice.

Anxiety-Like Behavior, Locomotor Response to Cocaine, and Thermoregulation Are Altered in $Pam^{Emx1\text{-}cKO/cKO}$ Mice. Based on the extensive literature on peptidergic signaling in the nervous system and the phenotypes observed in $Pam^{KO/+}$ mice, we first examined $Pam^{Emx1\text{-}cKO/cKO}$ mice. Previously, $Pam^{KO/+}$ mice exhibited a striking increase in anxiety-like behavior compared with WT mice (14, 39); this increase was largely ameliorated when the mice were fed a copper-supplemented diet. Anxiety-like behavior was tested using the elevated 0 maze (Fig. 3*A*). Unlike mice with a single allele of *Pam* in all of their tissues (Fig. 3*A*, red arrow), $Pam^{Emx1\text{-}cKO/cKO}$ mice showed an increase in time spent in the open arms of the maze, a response interpreted as a decrease in anxiety-like behavior. Anxiety-like behavior in $Pam^{Emx1\text{-}cKO/+}$ mice, with a single copy of *Pam* only in Emx1-positive cells, did not differ from control mice (Fig. 3*A*).

Studies from many laboratories have revealed a role for amidated peptides in cocaine self-administration and cocaine-seeking behavior during withdrawal (40–45). NPY, oxytocin, and the hypocretins (Hcrts; also called orexins) modulate these behaviors and are inactive if not amidated. We tested the response of $Pam^{Emx1\text{-}cKO/cKO}$ mice to 4 injections of cocaine, 4 d of abstinence, and a final injection of cocaine (Fig. 3*B*) (33). No difference was observed in the response of WT and $Pam^{Emx1\text{-}cKO/cKO}$ mice to the initial administration of saline (day 1). $Pam^{Emx1\text{-}cKO/cKO}$ mice exhibited a much greater response to the initial high dose of cocaine than WT mice (day 2); this increased responsiveness was maintained throughout the entire experimental protocol (RM-ANOVA; $P < 0.0001$).

Thermoregulation was studied, because the diminished ability of $Pam^{KO/+}$ mice to vasoconstrict peripheral blood vessels led to a marked inability to maintain core body temperature when kept at 4 °C (14); this deficit forced termination of the previous experiments after 2 h in the cold, when body temperature in $Pam^{KO/+}$ mice fell to 34 °C (Fig. 3*C*, red arrow). $Pam^{Emx1\text{-}cKO/cKO}$ mice outperformed control mice when maintained in a 4 °C environment for a prolonged period of time (Fig. 3*C*). In WT mice, body temperature fell significantly between 2 and 3 h of cold exposure; $Pam^{Emx1\text{-}cKO/cKO}$ mice were better able to maintain core body temperature for 3 h in a 4 °C environment (Fig. 3*C*). Since PAM expression is reduced to half in both excitatory and inhibitory neurons in $Pam^{KO/+}$ mice, while $Pam^{Emx1\text{-}cKO/cKO}$ mice lack PAM expression only in excitatory neurons, a difference in their ability to maintain core body temperature was anticipated. Excitatory neurons in the median preoptic area of the hypothalamus promote peripheral dilatation and core heat loss and produce a number of amidated peptides, which strongly affect thermoregulation (46, 47).

Excitatory Neurons in the Hippocampus and Cortex of $Pam^{Emx1\text{-}cKO/cKO}$ Mice Lack PAM. We used a reporter line in which a fluorescent marker, TdTomato, is produced in cells expressing Cre recombinase

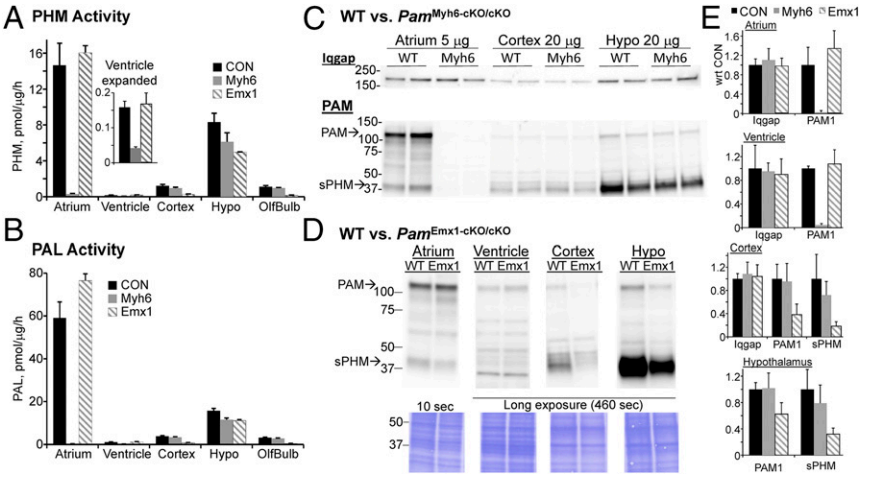

Fig. 2. Enzyme assays and western blots demonstrate tissue-specific elimination of PAM expression. PHM (*A*) and PAL (*B*) activity assays. Data, as picomoles of product produced per microgram of lysate protein per hour, are composites of 3 or more PHM assays and 2 or more PAL assays of lysates prepared from ≥6 mice. (*C*) Lysates from CON and $Pam^{Myh6\text{-}cKO/cKO}$ mice were subjected to western blot analysis using PAM exon 16 antibody; the samples shown were analyzed on the same gel using Iqgap as a loading control. The exposure time shown for the PAM antibody was 10 s; for the Iqgap antibody it was 460 s. (*D*) Lysates (20 μg protein, except atrium [5 μg]) prepared from the indicated tissues from WT and $Pam^{Emx1\text{-}cKO/cKO}$ mice were analyzed in the same manner, with equal loading demonstrated by Coomassie staining. (*E*) Western blot data for PAM-1 and soluble PHM (sPHM) were quantified from multiple gel sets, always loading equal protein as verified by the Iqgap signal; for each gel set, band intensities for knockout tissues were normalized with respect to (wrt) the corresponding WT band intensity, which was set to 1.00. Data from at least 3 different sample sets were quantified.

to verify the specificity of our knockout strategy at the cellular level (28). To evaluate the overlap between TdTomato-positive cells and PAM-positive cells, PAM was visualized using an antiserum specific for PAM-1 (Fig. 4); immunocytochemistry controls are presented in *SI Appendix*, Figs. S3 to S6. As expected (15), TdTomato expression was observed in pyramidal neurons in the cornu ammonis 1 (CA1) and CA3 regions of the hippocampus in Emx1-Cre recombinase mice (Fig. 4 *A*, *B*, yellow arrows, and *C*, yellow arrows). Since the TdTomato reporter is cytosolic, the axons and dendrites of TdTomato-expressing neurons were fluorescent. This was especially apparent in the CA3 region, where a significant fraction of the granule cell mossy fiber (mf) endings innervating the dendrites of the CA3 pyramidal neurons were bright red (Fig. 4*C*, mf).

Consistent with our previous in situ hybridization study (15), the vast majority of pyramidal neurons in both the CA1 and CA3 regions of the hippocampus expressed PAM (AlexaFluor488; green) (Fig. 4 *B*, yellow arrows and *C*, yellow arrows); PAM staining was also strong in the mfs. Large, strongly PAM-positive neurons that were not TdTomato positive were scattered throughout the pyramidal cell layer in CA1 and CA3 and in the stratum oriens and stratum lacunosum moleculare (Fig. 4 *B*, green arrows and *C*, green arrows).

In layer 2 of the cerebral cortex (Fig. 4*D*), all of the TdTomato-expressing neurons (Fig. 4*D*, red) were PAM positive (Fig. 4*D*, yellow arrows), suggesting that most of the excitatory neurons in cortical layer 2 could utilize amidated peptides for signaling. PAM staining in the TdTomato-positive pyramidal projection neurons in cortical layer 5 was less intense, but all of the TdTomato-positive neurons expressed PAM (Fig. 4*E*, yellow arrows). The layer 5 neurons with the most intense PAM signal were not TdTomato positive, suggesting that they were interneurons (Fig. 4*E*, green arrows).

The number of neurons in layers 2 and 5 expressing TdTomato and stained for PAM and the number of PAM-positive neurons not expressing TdTomato were compared with the total number of nuclei (Fig. 4*F*). In both layers, the number of neurons expressing PAM but not expressing TdTomato were approximately 1/5th of the number of neurons expressing both PAM and TdTomato.

PAM Is Highly Expressed in GAD67-Positive Interneurons. Given the importance of excitatory/inhibitory balance in nervous system function, we wanted to identify PAM-positive inhibitory neurons; to do so, coronal sections from control and $Pam^{Emx1\text{-}cKO/cKO}$ mice were stained simultaneously for PAM (Fig. 5, green) and GAD67 (Fig. 5, red). The strongly PAM-positive neurons seen in the stratum oriens and stratum lacunosum moleculare of the CA3 region in both control and $Pam^{Emx1\text{-}cKO/cKO}$ mice were largely GAD positive (Fig. 5*A*, yellow arrows). Strikingly, the PAM-positive mfs observed in the WT CA3 region were not seen in the $Pam^{Emx1\text{-}cKO/cKO}$ brain (Fig. 5*B*). In WT mice, NPY, an amidated peptide, is highly expressed in mfs (29). The diffuse nature of the green AlexaFluor488 signal observed in pyramidal neurons in the $Pam^{Emx1\text{-}cKO/cKO}$ mice (Fig. 5*B*) resembled the background observed when PAM antibody was replaced by nonimmune rabbit immunoglobulin (Ig) or blocked with antigenic peptide (*SI Appendix*, Figs. S4 to S7).

In cortical layer 2 (Fig. 5 *C* and *D*), very few PAM-positive neurons were identified in $Pam^{Emx1\text{-}cKO/cKO}$ mice; almost all of the remaining PAM-positive neurons expressed GAD67 (inhibitory neurons) (Fig. 5*D*, yellow arrow and *SI Appendix*, Figs. S6 and S7). The PAM-positive neurons in cortical layer 5 of $Pam^{Emx1\text{-}cKO/cKO}$ mice (Fig. 5*E*, yellow arrow) were almost always GAD67 positive (inhibitory) (*SI Appendix*, Figs. S6 and S7). In the cerebral cortices of WT mice, there were PAM-positive neurons not positive for GAD as expected from the majority of PAM-positive neurons that were Emx1 positive (Fig. 5, white arrows). In addition, in $Pam^{Emx1\text{-}cKO/cKO}$ mice, there were PAM-positive neurons that were not GAD positive (Fig. 5*E*, white arrows). The decreases in PAM-positive neuron numbers in cortical layers 2 and 5 in $Pam^{Emx1\text{-}cKO/cKO}$ mice (layer 2: 56%; layer 5: 39%) closely matched the numbers of neurons expressing both PAM and TdTomato in the Emx1-Cre reporter mice (layer 2: 56.0 ± 9.5%; layer 5: 44.3 ± 6.4%) (summarized in *SI Appendix*, Table S2).

Anxiety-Like Behavior and Thermoregulation Are Altered in $Pam^{Myh6\text{-}cKO/cKO}$ Mice. Although atrial levels of PAM are at least 10-fold higher than cortical levels (18) (Fig. 2), neither proANP nor probrain natriuretic peptide (proBNP) is amidated. The tests used to characterize $Pam^{Emx1\text{-}cKO/cKO}$ mice (Fig. 3) were also used to evaluate $Pam^{Myh6\text{-}cKO/cKO}$ mice (Fig. 6). When tested for anxiety-like behavior, the $Pam^{Myh6\text{-}cKO/cKO}$ mice responded in much the same way as $Pam^{KO/+}$ mice; time spent in the open arms decreased to about half of the value observed in control mice (Fig. 6*A*). The anxiety-like behavior of $Pam^{Myh6\text{-}cKO/+}$ mice did not differ from that of control mice. When tested using the cocaine injection paradigm described in Fig. 3*B*, $Pam^{Myh6\text{-}cKO/cKO}$ mice showed an enhanced response only on day 2 ($P < 0.02$); unlike $Pam^{Emx1\text{-}cKO/cKO}$ mice, the elevated response was not sustained (Fig. 6*B*). Like $Pam^{Emx1\text{-}cKO/cKO}$ mice, $Pam^{Myh6\text{-}cKO/cKO}$ mice were better able than WT mice to maintain core body temperature for 3 h in a 4 °C environment (Fig. 6*C*).

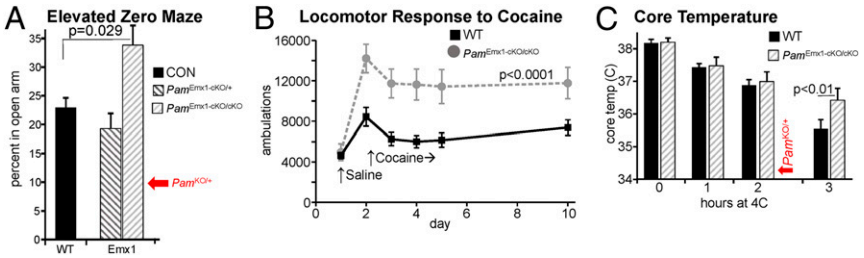

Fig. 3. Behavioral/physiological tests of $Pam^{Emx1\text{-}cKO/cKO}$ mice. (*A*) Anxiety-like behavior. Mice ranged from 60 to 88 d old: CON, $n = 48$; $Pam^{Emx1\text{-}cKO/+}$, $n = 24$; and $Pam^{Emx1\text{-}cKO/cKO}$, $n = 24$. Data for global *Pam* heterozygotes ($Pam^{KO/+}$) derived from Emx1-Cre parents (this work) did not differ from data obtained in our previous study (red arrow; $Pam^{KO/+}$) (14). (*B*) Locomotor response to cocaine. Ambulations were recorded for 45 min after an i.p. injection of saline (day 1) or cocaine (20 mg/kg on day 2; 10 mg/kg on days 3, 4, 5, and 10). Mice ranged from 68 to 151 d old: WT, $n = 8$; and $Pam^{Emx1\text{-}cKO/cKO}$, $n = 8$. Repeated-measures ANOVA was used to compare knockout to WT. (*C*) Core body temperature. Temperature was measured using a rectal thermometer: WT, $n = 10$; and $Pam^{Emx1\text{-}cKO/cKO}$, $n = 20$. Mice ranged from 67 to 134 d old. Student *t* test applied for the 3-h data. Previous data from global *Pam* heterozygotes ($Pam^{KO/+}$) are shown by the red arrow ($Pam^{KO/+}$) (14).

The marked improvement in the ability of the $Pam^{Myh6\text{-}cKO/cKO}$ mice to maintain core body temperature for 3 h suggested that these mice had an enhanced coping mechanism whereby they could redirect peripheral blood flow to the core (34, 35). A common test for this ability is use of a heat-sensitive probe to monitor tail temperature while the animal is kept in an unaccustomed restraint device for 20 min (34, 35); abdominal temperature is measured with the same probe before and after the 20-min restraint, and the temperature differential (abdomen minus tail) is reported (Fig. 6*D*). Measured in this manner, abdominal temperature was the same in $Pam^{Myh6\text{-}cKO/cKO}$ and WT mice both before and after restraint. The tail temperature differential was significantly greater in $Pam^{Myh6\text{-}cKO/cKO}$ mice than in WT mice after 20 min of restraint, indicating an enhanced ability of $Pam^{Myh6\text{-}cKO/cKO}$ mice to constrict tail blood flow.

Atrial Levels of ProANP Decline in $Pam^{Myh6\text{-}cKO/cKO}$ Mice. As expected from the literature (19, 20) and consistent with the dramatically reduced levels of PAM protein and enzyme activity measured in the atria and ventricles of $Pam^{Myh6\text{-}cKO/cKO}$ mice (Fig. 2), TdTomato was uniformly expressed in atrial and ventricular cardiomyocytes when driven by the Myh6 promoter (*SI Appendix*, Fig. S7).

Unlike pituitary and neuronal secretory granules, PAM is the major protein in the membranes of atrial secretory granules, which store proANP and proBNP (7, 48–50). In addition, PAM interacts directly with proANP, which is not cleaved until the time of secretion (24, 51). Lysates prepared from WT and $Pam^{Myh6\text{-}cKO/cKO}$ atria using 1% deoxycholate to ensure better protein solubilization were subjected to western blot analysis (Fig. 7*A*). As assessed using antibodies to PAM exon 16 (JH629) and to the cytoplasmic domain of PAM (C-Stop), PAM levels in $Pam^{Myh6\text{-}cKO/cKO}$ atria were negligible. ANP levels were assessed using an antibody specific for the N-terminal region of proANP and an antibody specific for a 15-residue peptide contained within mature 28-residue ANP. Both antibodies revealed a dramatic drop in proANP levels in $Pam^{Myh6\text{-}cKO/cKO}$ atria (Fig. 7*A*).

To determine whether the decline in proANP levels in the atria of $Pam^{Myh6\text{-}cKO/cKO}$ mice was accompanied by altered circulating levels of ANP, we utilized an ELISA to quantify atrial and serum levels of ANP in $Pam^{Myh6\text{-}cKO/cKO}$ and WT mice (Fig. 7*B*). Levels of ANP in the atria and sera of $Pam^{Myh6\text{-}cKO/cKO}$ mice were dramatically lower than in control mice. Although PAM expression in the atrium exceeds levels in any other tissue examined, levels of serum PHM activity were unaltered in $Pam^{Myh6\text{-}cKO/cKO}$ mice (Fig. 7*C*), eliminating the atrium as a major source of serum PAM.

Blood Pressure Regulation Is Altered in $Pam^{Myh6\text{-}cKO/cKO}$ Mice. ANP has been referred to as a natural antihypertensive agent (52); along with several other peptides, ANP participates in the control of blood pressure and the ability of mammals to respond to changes in dietary salinity and cardiovascular fluid volume (37, 53–55). Since circulating levels of ANP were undetectable in $Pam^{Myh6\text{-}cKO/cKO}$ mice, their ability to regulate blood pressure in response to a change in dietary salt load was examined. When fed a normal salt diet (0.49% NaCl) for 2 mo, no differences in blood pressure were observed between control and $Pam^{Myh6\text{-}cKO/cKO}$ mice (Fig. 7*D*, day 0); blood pressure was consistently slightly higher in female mice than in male mice, irrespective of PAM genotype.

This result suggested that other systems might be compensating for the low levels of ANP in $Pam^{Myh6\text{-}cKO/cKO}$ mice. The renin-angiotensin system increases blood pressure by stimulating the conversion of angiotensinogen to angiotensin I; renin secretion is stimulated by low blood sodium and sympathetic input and suppressed by ANP (56). However, assays for serum renin levels in WT and $Pam^{Myh6\text{-}cKO/cKO}$ mice on a normal salt diet revealed no difference (Fig. 7*E*).

The WT and $Pam^{Myh6\text{-}cKO/cKO}$ mice, in which blood pressure was monitored after 2 mo on a normal salt diet, were fed a high-salt diet (8% NaCl) for a week (Fig. 7*D*) (days 4 to 10). No changes in blood pressure or body weight were observed, despite the low levels of ANP found in $Pam^{Myh6\text{-}cKO/cKO}$ mice. These mice were then returned to the normal salt diet (days 11 to 18), again with no changes observed in blood pressure.

The sympathetic system, a major ANP target (37, 57), plays an essential role in blood pressure control. Hexamethonium, a ganglionic blocker that eliminates all presynaptic sympathetic ganglion input, was used to test the hypothesis that sympathetic tone differed in WT and $Pam^{Myh6\text{-}cKO/cKO}$ mice (37, 38, 58). As expected, control mice exhibited an ∼20-mm Hg decrease in arterial blood pressure 10 min after an injection of hexamethonium (Fig. 7*F*). In contrast, blood pressure in $Pam^{Myh6\text{-}cKO/cKO}$ mice was unaltered after hexamethonium injection, revealing a striking absence of sympathetic tone.

The Transcriptome Is Altered in *Pam* $^{Myh6\text{-}cKO/cKO}$ Atrium. The homogeneity of atrial tissue, lack of a major amidated product despite high levels of *Pam* expression, and changes observed in the $Pam^{Myh6\text{-}cKO/cKO}$ mice led us to ask whether changes in gene expression might contribute to the phenotypes observed. Alterations in the atrial transcriptome could reflect the inability of these cells to produce soluble fragment of the peptidylglycine α-amidating monooxygenase cytosolic domain (sfCD; which translocates to the nucleus) (25), a direct response to the diminished levels of ANP or compensatory responses by the many systems involved in regulating these fundamental processes. Atrial RNA was prepared from WT and $Pam^{Myh6\text{-}cKO/cKO}$ mice and sequenced (Fig. 8*A* and Dataset S1).

DESeq2 analysis of differential expression was performed on the counts data, yielding 1,063 transcripts with $P < 0.05$; when outliers were eliminated (33), the number of differentially expressed transcripts dropped to 555. When depicted as a volcano plot, the vast majority of over 14,000 transcripts with average fragments per kilobase of transcript per million mapped reads (FPKM) > 1 were clustered near the origin, with a WT/knockout ratio within the 0.5 to 2.0 range ($\log_2$[ratio] −1 to +1) and a DESeq2 *P* value > 0.05.

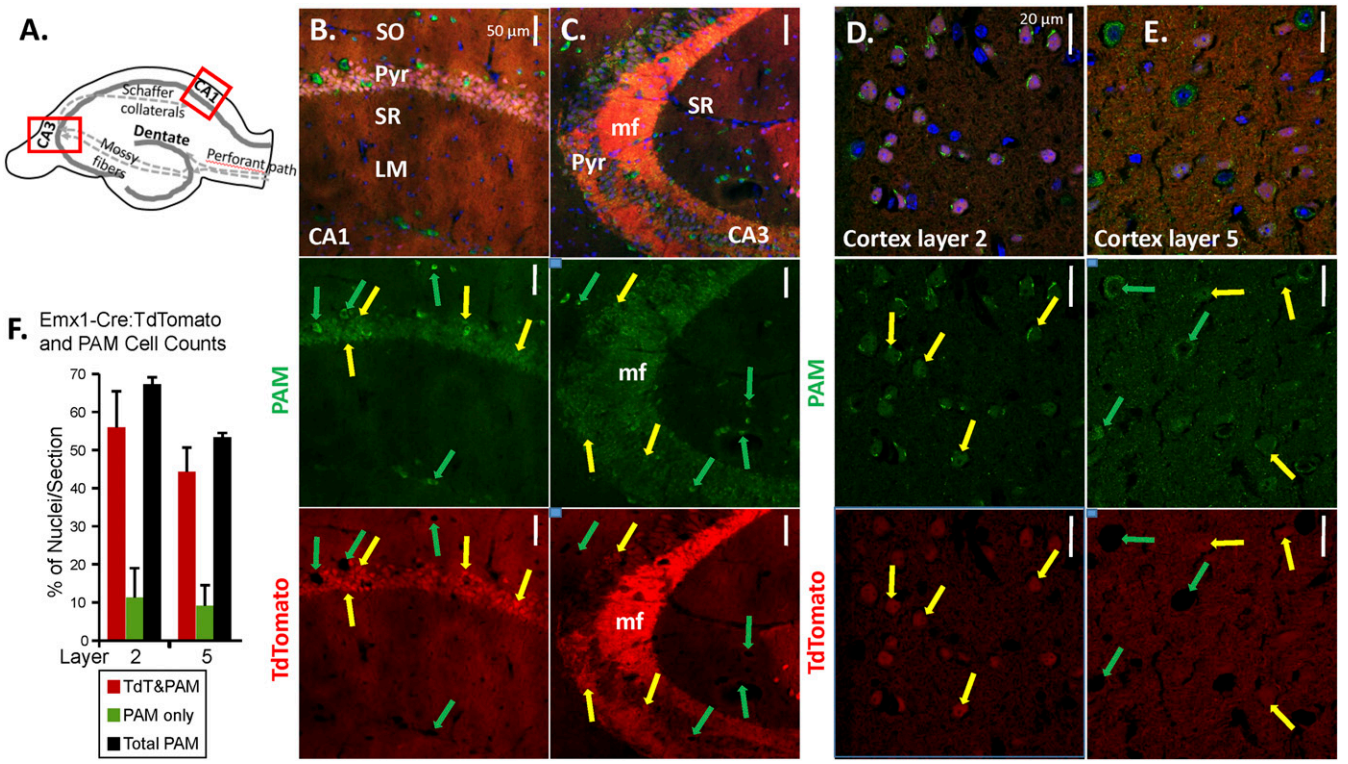

Fig. 4. PAM is expressed in all Emx1-expressing (excitatory) neurons. Adult mice expressing a TdTomato Cre-reporter construct and Emx1-Cre were perfusion fixed; coronal sections were stained for PAM using affinity-purified exon 16 antibody and AlexaFluor488-tagged secondary antibody (green), while nuclei were visualized using Hoechst stain (blue). Images shown are single-plane confocal images. (*A*) Diagram of the hippocampus and major pathways; boxed areas indicate the regions of CA1 and CA3 examined. (*B*) CA1 region. (*C*) CA3 region. (*D*) Cortex layer 2. (*E*) Cortex layer 5. All TdTomato-positive neurons were also PAM positive (yellow arrows). A fraction of the PAM-positive neurons did not express TdTomato (green arrows). LM, lacunosum moleculare; Pyr, stratum pyramidale; SO, stratum oriens; SR, stratum radiatum. (Scale bars, 50 μm [hippocampus]; 20 μm [cortex].) (*F*) Cell counts. Cortical images from 2 mice were quantified (4 to 5 images per region per animal, 141 to 213 nuclei per layer per animal): the number of TdTomato/PAM-positive cells and TdTomato-negative/PAM-positive cells is expressed as a percentage of nuclei (Hoechst stained).

The 555 significantly altered transcripts were subjected to Ingenuity Pathway Analysis (IPA) (Fig. 8 *B* and *C* and *SI Appendix*, Fig. S8) (33). One of the most significantly regulated networks identified by IPA was the Apelin network. Apelin (Gene ID 8862) is an adipokine made in the atrium in which FPKM level rose 2.6-fold in $Pam^{Myh6\text{-}cKO/cKO}$ mice compared with WT. Apelin is used clinically to treat insulin resistance and hypertension (59). Another major network includes a set of transcripts involved in circadian rhythms (3 period genes: *Clock*, *Bhlhe40[Dec1]*, and *Arntl[Bmal1]*). Bhlhe40 is a basic helix–loop–helix protein, which binds to the promoter of *Per1* to repress Clock/Arntl activation of *Per1*; Bhlhe40 levels vary directly with blood pressure in Clock knockout mice (60). Three more significantly regulated networks identified by IPA are depicted in *SI Appendix*, Fig. S8. The tight interconnections of these 5 predicted networks are striking, with several transcripts appearing in 2 or 3 of the 5 networks: Apln, Apold1, Gadd45b, Bhlhe40, and Per1.

Many of the differentially expressed atrial transcripts were also identified as *Pam*-regulated genes in pituitary corticotrope cells (10) (*SI Appendix*, Table S3). Strikingly, 29 of 40 atrial transcripts in the 5 most significantly regulated networks responded to changes in *Pam* expression in the same manner in these 2 very different systems (marked with asterisks in Fig. 8 *B* and *C*). For example, expression of *Per1* increased more than 2-fold in $Pam^{Myh6\text{-}cKO/cKO}$ mice compared with WT and decreased to 60% when *Pam* expression was increased in pituitary cells (10), suggesting that the change may be a direct response to altered PAM levels. Expression of 10 atrial transcripts (marked with X in Fig. 8 *B* and *C*) decreased with loss of atrial PAM and also decreased in pituitary cells when PAM was increased (10), suggesting that these transcripts are not responding directly to the PAM protein but rather to some other compensatory changes or differences between the 2 tissues. Five of 39 atrial transcript are not expressed at significant levels in pituitary cells (marked with 0 in Fig. 8 *B* and *C*).

Discussion

Rationale. Peptidergic signaling in species as diverse as *Trichoplax*, *Drosophila*, and human shares many common features (8). The preproproteins synthesized into the lumen of the ER undergo a series of posttranslational modifications that generate a wide variety of products. In many cases, these modifications are tissue specific and generate multiple products that can interact with different receptors. The receptors, which are almost always GPCRs, may be located nearby or far away. Peptides play essential roles in the organism's response to nutrients and to noxious stimuli, function to distinguish self from nonself, participate in sexual reproduction, and control motility through their effects on ciliary beating and muscle contractility. Peptide expression is regulated at multiple levels, with changes in transcription, translation, and posttranslational processing as well as acute effects on peptide release. This complexity has made it difficult to utilize specific peptides in the development of therapeutics.

To test the utility of $Pam^{cKO/cKO}$ mice in revealing functionally significant effects of peptidergic signaling, we selected 2 Cre drivers. Based on the widespread expression of PAM throughout the nervous system (Figs. 4 and 5) (15), we utilized the Emx1-Cre mouse. The fact that cortical PAM activity fell to 25% of control

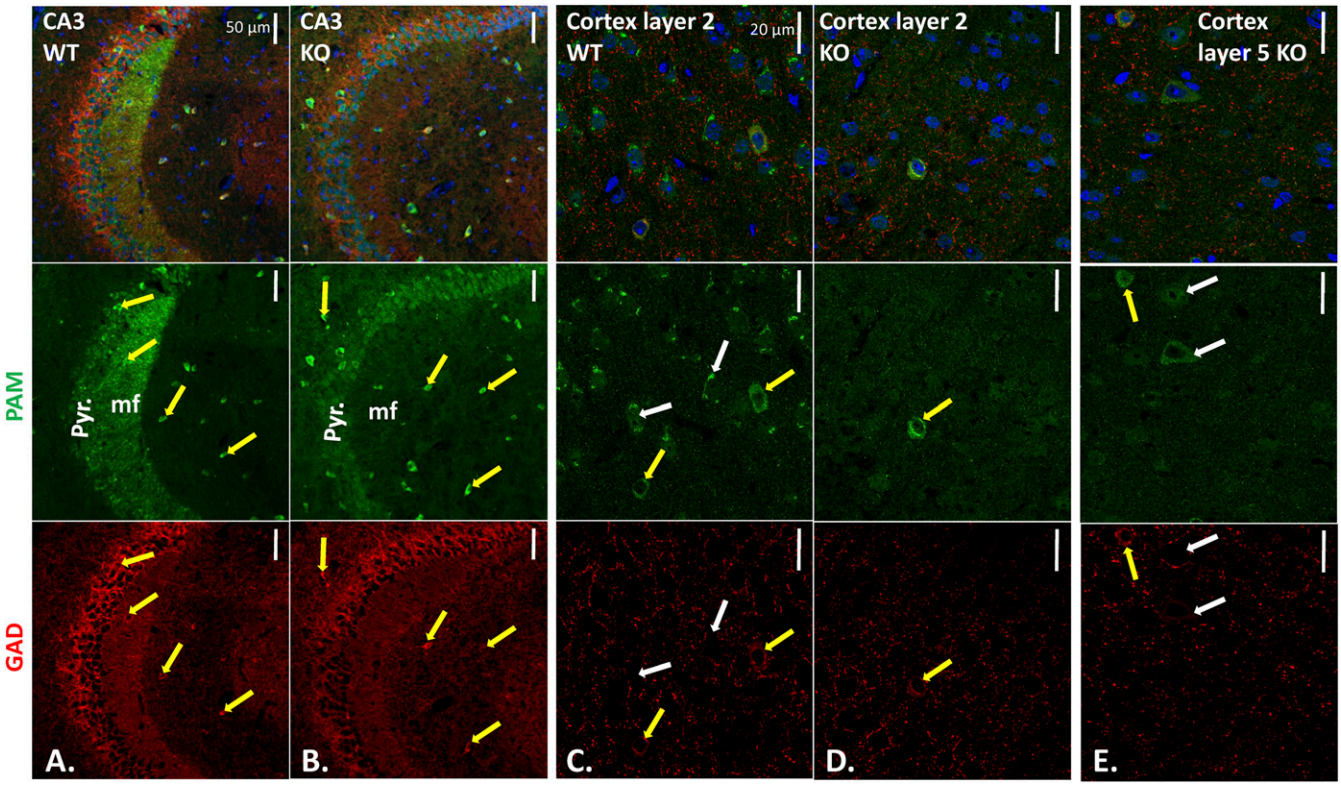

Fig. 5. Many of the PAM-positive neurons that remain in the hippocampus and cortex of $Pam^{Emx1\text{-}cKO/cKO}$ mice express GAD. Sections stained with affinity-purified PAM exon 16 antibody plus AlexaFluor488 antibody to rabbit IgG (green), mouse monoclonal antibody to GAD67 plus Cy3 antibody to mouse IgG (red), and Hoechst nuclear stain (blue). CA3 regions of WT (*A*) and knockout (KO) (*B*) hippocampus; yellow arrows mark neurons stained for PAM and GAD67. WT (*C*) and KO (*D*) layer 2 and KO layer 5 (*E*) visualized as described for hippocampus In KO layer 2, all GAD-positive neurons were PAM positive; in KO layer 5, some PAM-positive neurons were not GAD positive (white arrows). Quantification is in *SI Appendix*, Table S2. Pyr, stratum pyramidale. (Scale bars, 50 μm [hippocampus]; 20 μm [cortex].)

values in the cortices of $Pam^{Emx1\text{-}cKO/cKO}$ mice is consistent with the prevalence of excitatory neurons (Fig. 2). A proper balance of excitatory and inhibitory inputs is critical to the functioning of many circuits, and we hypothesized that loss of PAM in excitatory neurons would disrupt this balance. Eliminating the expression of vasoactive intestinal polypeptide, an amidated peptide, in inhibitory interneurons in the auditory cortex alters acoustic gain (61). In the feeding–satiety network, different sets of neurons, many producing amidated peptides, function in a dynamic balance (62). The Myh6-Cre mouse was selected to gain insight into potential nonenzymatic roles played by PAM in atrial myocytes, which produce massive amounts of PAM (18, 48, 49), despite the fact that neither of their major peptide products, ANP and BNP, is amidated; atrial PAM levels fell to <2% of control in $Pam^{Myh6\text{-}cKO/cKO}$ mice (Fig. 2). Atrial myocytes store intact proANP in secretory granules in which the major membrane protein is PAM (48, 49).

Immunostaining readily identified PAM in every TdTomato-positive neuron (Fig. 4). This observation is consistent with the 4-fold drop in PHM and PAL activity observed in the cortices of the $Pam^{Emx1\text{-}cKO/cKO}$ mice (Fig. 2). A subset of the gamma aminobutyric acid-positive neurons expressed PAM; in general, PAM staining in GABAergic neurons was more intense than in other neurons. Mice entirely lacking the ability to express PAM did not survive beyond E14.5 (11), with massive edema accompanied by a poorly formed vasculature. Surprisingly, mice lacking the ability to express PAM only in their cardiomyocytes did not exhibit these defects. $Pam^{Myh6\text{-}cKO/cKO}$ mice grew normally, performed as well as WT mice on the rotarod and in the open field, and outperformed WT mice in thermoregulation tests.

Anxiety-Like Behavior. The amygdala plays a crucial role in anxiety (63). Anxiety-like behavior increased in $Pam^{KO/+}$ mice, with reduced levels of PAM expression in both excitatory and inhibitory neurons (14). In contrast, eliminating *Pam* expression only in excitatory neurons resulted in a decrease in anxiety-like behavior (Fig. 3*A*). Treatment of $Pam^{KO/+}$ mice with diazepam, a GABA-A receptor agonist, normalized their anxiety-like behavior, suggesting that it resulted from limited inhibitory tone (14, 39). Ifenprodil, which blocks a subtype of excitatory glutamate receptors, has anxiolytic actions in WT mice (64). If the net effect of the amidated peptides expressed in excitatory neurons is to facilitate the actions of glutamate, eliminating their expression in $Pam^{Emx1\text{-}cKO/cKO}$ mice would also be expected to reduce anxiety-like behavior as observed (Fig. 3*A*). The peptides in which lack of amidation is most likely to contribute to reduced excitatory output in the $Pam^{Emx1\text{-}cKO/cKO}$ mice are the Hcrts, oxytocin, NPY, and cholecystokinin (40, 41, 45, 65–67). The deficits observed in the $Pam^{Emx1\text{-}cKO/cKO}$ mice indicate that further study is warranted given the large number of neuropeptides and receptors involved, the complexity of the circuits, and the lack of specific pharmacological blockers.

The increase in anxiety-like behavior observed in $Pam^{KO/+}$ mice was mimicked in the atrium-specific total knockout $Pam^{Myh6\text{-}cKO/cKO}$ mice (Fig. 6*A*). Both the reduction in atrial and circulating ANP levels and the alterations in atrial gene expression observed in $Pam^{Myh6\text{-}cKO/cKO}$ mice may contribute to this phenotype; it is not yet clear whether the enzymatic activity of PAM plays a role. There is a well-recognized correlation between high anxiety and low circulating ANP levels in human cardiovascular patients (68); a subset of patients with low anxiety have high circulating

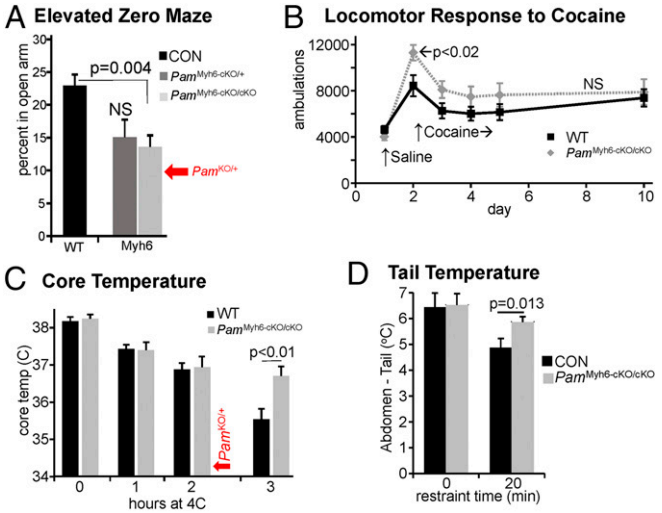

Fig. 6. Behavioral/physiological tests of $Pam^{Myh6\text{-}cKO/cKO}$ mice. $Pam^{Myh6\text{-}cKO/cKO}$ mice were tested along with the mice reported in Fig. 3; control data are replicated here. (*A*) Anxiety-like behavior. Mice ranged from 60 to 88 d old: CON, $n = 48$; $Pam^{Myh6\text{-}cKO/+}$, $n = 20$; and $Pam^{Myh6\text{-}cKO/cKO}$, $n = 30$. Data obtained previously for $Pam^{KO/+}$ are shown (red arrow) (14). (*B*) Locomotor response to cocaine. Ambulations after an i.p. injection of saline or cocaine were recorded as described in Fig. 3. Mice ranged from 61 to 114 d old: WT, $n = 8$; and $Pam^{Myh6\text{-}cKO/cKO}$, $n = 12$. Repeated-measures ANOVA was used to compare knockout to CON. (*C*) Core body temperature: WT, $n = 10$; and $Pam^{Myh6\text{-}cKO/cKO}$, $n = 10$. Mice ranged from 67 to 134 d old. Student *t* test applied for the 3-h data. Previous data for $Pam^{KO/+}$ are shown by the red arrow (14). (*D*) Abdominal and tail temperatures during 20-min restraint in an unfamiliar environment. Abdominal temperatures were determined at the beginning and end of 20-min restraint, and tail temperatures were determined throughout the experiment. The differences (abdomen minus tail) at 0 and 20 min are shown: CON, $n = 20$; and $Pam^{Myh6\text{-}cKO/cKO}$, $n = 23$. NS, not significant.

levels of the N-terminal proANP (69). It is striking that a number of transcripts, which could adversely affect cardiac function, were altered in $Pam^{Myh6\text{-}cKO/cKO}$ mice, potentially contributing to anxiety: increased Hdac4, promoting myocardial ischemia; increased Prkag2, lowering heart rate; increased Usp2, blunting mineralocorticoid responsiveness and decreasing retention of high salt; and decreased Ano1 (a Ca^{2+}-activated Cl^- channel) and increased Cacna1a (Ca^{2+} channel), both potentially increasing the strength of heart contraction.

Response to Cocaine. The locomotor response to cocaine involves altered signaling in the nucleus accumbens, with established roles for dopamine, glutamate, and amidated neuropeptides, such as NPY, oxytocin, and the Hcrts (65–67). Activation of the NPY Y1 receptor in the amygdala increases self-administration of psychostimulants, such as cocaine, while activation of the NPY Y2 receptor inhibits self-administration (40, 45). Hcrt1 and Hcrt2 are amidated peptides derived from adjacent regions of the Hcrt precursor. The Hcrtr1 receptor binds Hcrt1 much better than Hcrt2 (41), and selective inhibitors of Hcrtr1 receptors are in clinical trials to treat cocaine addiction (41). Systemic delivery of oxytocin reduces cocaine self-administration (44) (also in clinical trials). The antiaddictive actions of oxytocin, NPY (at the Y2 receptor), and Hcrts (at Hcrtr2) could be missing in $Pam^{Emx1\text{-}cKO/cKO}$ mice (Fig. 3*B*) but not in $Pam^{Myh6\text{-}cKO/cKO}$ mice (Fig. 6*B*).

Thermoregulation. $Pam^{Emx1\text{-}cKO/cKO}$ mice withstand cold exposure better than WT mice (Fig. 3*C*). The preoptic area of the hypothalamus is the central control region for core body temperature (47). Glutamatergic (excitatory, Emx1-expressing) neurons drive peripheral dilatation and severe hypothermia (46), while GABAergic neurons have less effect (70). Excitatory neurons in the preoptic area express many amidated neuropeptides: PACAP, CCK, CRH, oxytocin, tachykinin1, and GnRH (47, 71). Importantly, ablation of medial preoptic excitatory neurons causes dramatic hyperthermia (46, 72); deletion of PAM in these neurons (as for ablation) could produce peripheral vasoconstriction and core heat gain.

$Pam^{Myh6\text{-}cKO/cKO}$ mice also withstand cold exposure better than WT mice (Fig. 6*C*). The RNAseq results provide potential explanations for this, with markedly increased transcript levels of growth arrest and DNA-damage-inducible 45 gamma (also called Ddit2) and decreased protein kinase, cAMP dependent regulatory, type 2 beta. Both changes could increase the expression of uncoupling protein 1, which is thermogenic, increasing metabolic rate. In addition, $Pam^{Myh6\text{-}cKO/cKO}$ mice were more capable than WT mice of decreasing heat loss from the periphery (tail, limbs) under stress (restraint or cold room) (Fig. 6*D*).

Blood Pressure. $Pam^{Myh6\text{-}cKO/cKO}$ mice showed no increase in blood pressure in response to salt loading (8% NaCl diet), matching WT mice (Fig. 7*D*). Use of hexamethonium revealed that 20 mm Hg of the WT mouse blood pressure was due to resting sympathetic nervous tone, while $Pam^{Myh6\text{-}cKO/cKO}$ mice lacked any resting sympathetic tone (Fig. 7*F*). The absence of any TdTomato signal in the superior cervical ganglia of $Pam^{Myh6\text{-}TdTomato}$ mice coupled with barely detectable Myh6 messenger RNA (mRNA) levels (73) suggests that PAM expressed in the sympathetic ganglia of $Pam^{Myh6\text{-}cKO/cKO}$ mice would be producing bioactive NPY, a potent vasoconstrictor. $Pam^{Myh6\text{-}cKO/cKO}$ mice have negligible circulating ANP (Fig. 7*B*) as do ANP and Corin knockout mice, which exhibit salt-induced hypertension of 15 to 30 mm Hg (27, 37, 74). ANP and BNP are released from the atrium in response to cardiac distension (37, 53). WT mice fed solid diets containing 0.49% (normal) and 8% (high) NaCl show no detectable elevation in arterial blood pressure in most studies (27, 37, 74); only 25% of normotensive humans are salt sensitive by the American Heart Association (75).

ANP, vasopressin, angiotensin II, bradykinin, and NPY are the dominant peptides controlling blood pressure responses to dietary salt and altered cardiovascular volume (37, 53, 55). Only vasopressin and NPY require amidation for bioactivity, and both elevate blood pressure; therefore, loss of amidation could decrease blood pressure. ANP works in opposition to the sympathetic system, attenuating vascular tone, inhibiting vasopressin release, reducing renin release, and decreasing angiotensinogen conversion into angiotensin (37, 53, 55). Since circulating renin levels were unaltered in $Pam^{Myh6\text{-}cKO/cKO}$ mice (Fig. 7*E*), we hypothesize that lack of sympathetic tone (Fig. 7*F*) counterbalances loss of circulating ANP (Fig. 7*C*).

ANP Levels. ANP levels in the atria and sera of $Pam^{Myh6\text{-}cKO/cKO}$ mice fell dramatically. Although ANP is not amidated, PAM levels in the atrium exceed those in any other tissue. ProANP and PAM, the major proteins in atrial secretory granules, interact with each other (48, 49, 76), raising the possibility that atrial granules fail to form normally due to the absence of PAM. Phylogenetic analyses indicate that natriuretic peptides (NPs) are ancient. While ANP and BNP predominate in the heart, C-type natriuretic peptide (CNP) is synthesized widely, with highest levels in the brain (77). An ancestral CNP was duplicated in elasmobranchs, with mammalian ANP and BNP derived from CNP3 (77). Elasmobranch CNP3 is a close relative of the single NP in hagfish, which is reported to have an amidated C terminus (77). The sequences of all teleost ANPs include a potential C-terminal amidation site (77) (NM_198800.3). However, crystallographic studies of the interactions between mammalian ANP or BNP and the dimerized receptor that binds a single ligand revealed no role for the NP C terminus (78, 79).

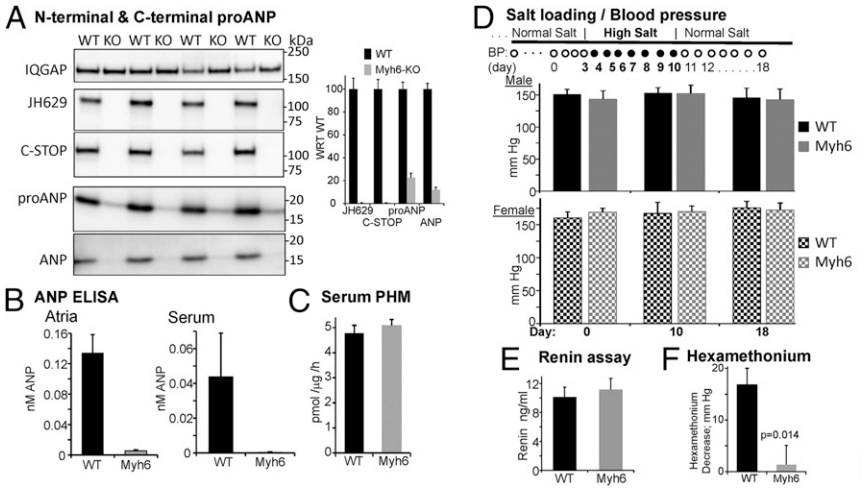

Fig. 7. Alterations in proANP and blood pressure regulation in *Pam*$^{Myh6\text{-}cKO/cKO}$ mice. (*A*) RIPA lysates of 4 pairs of WT and *Pam*$^{Myh6\text{-}cKO/cKO}$ atria (1 μg protein per lane) were fractionated by SDS/PAGE and analyzed for PAM (PAM-1–specific antibody JH629; PAM cytosolic domain antibody, C-Stop) and proANP; the gel that was analyzed using the ANP-specific and Iqgap antibodies had 10 μg protein per lane. Graph shows quantification relative to WT. WRT, with respect to. (*B*) ANP ELISAs confirmed the drop in ANP levels in atrial extracts and trunk blood ($n = 10$ for serum, $n = 14$ for tissue). (*C*) PHM assays on serum samples from WT and *Pam*$^{Myh6\text{-}cKO/cKO}$ mice (WT, $n = 3$; *Pam*$^{Myh6\text{-}cKO/cKO}$, $n = 3$). Similar results were obtained in a second assay comparing these mice as well as sera from WT and *Pam*$^{Emx1\text{-}cKO/cKO}$ mice (not shown). (*D*) High-salt diet. Tail cuff blood pressure was recorded for WT mice (5 male, 3 female) and *Pam*$^{Myh6\text{-}cKO/cKO}$ mice (3 male, 5 female). Mice were maintained for >2 mo on a normal salt diet (0.49% NaCl) and 7 d on a solid diet including 8% NaCl (high salt), during which body weight and food consumption remained constant, followed by an additional week on the normal salt diet. Mice were 79 to 101 d old. The experiment was repeated with WT mice (2 male, 2 female) and *Pam*$^{Myh6\text{-}cKO/cKO}$ mice (2 male, 2 female) with the same results. (*E*) Serum renin was measured by ELISA with 16 WT and 16 *Pam*$^{Myh6\text{-}cKO/cKO}$ samples. (*F*) Tail cuff blood pressure was recorded 10 min after an injection of isotonic saline (day 1) and after an injection of hexamethonium (day 2) (37, 38). The average difference between the days 1 and 2 data for each mouse is plotted. Fourteen WT mice and 15 *Pam*$^{Myh6\text{-}cKO/cKO}$ mice, 59 to 102 d old. BP, blood pressure; KO, knockout.

Perhaps what now seems to be a packaging role for PAM emerged from an earlier need for amidation.

Transcript Changes in Atria of *Pam*$^{Myh6\text{-}cKO/cKO}$ Mice. Levels of about 550 atrial transcripts were significantly altered in *Pam*$^{Myh6\text{-}cKO/cKO}$ mice (Fig. 8, *SI Appendix*, Fig. S8 and Table S3, and Dataset S1), just over 2% of the genome. Altered transcript levels may underlie some of the physiological changes seen in *Pam*$^{Myh6\text{-}cKO/cKO}$ mice, such as increased anxiety, heightened ability to withstand a cold challenge, and lack of increased blood pressure on an 8% NaCl diet (Figs. 6 and 7). One interesting transcript increased in *Pam*$^{Myh6\text{-}cKO/cKO}$ mice encodes preproapelin. Signal peptide removal yields proapelin, the 55-amino acid precursor to apelin, which is a nonamidated 13-amino acid peptide that binds to the apelin receptor APJ, gene symbol APLNR. Strikingly, the furin-like cleavage that generates apelin would be expected to produce an N-terminal peptidylglycine substrate that could be converted into an amidated 35-amino acid product by PAM. As observed for many prohormones,

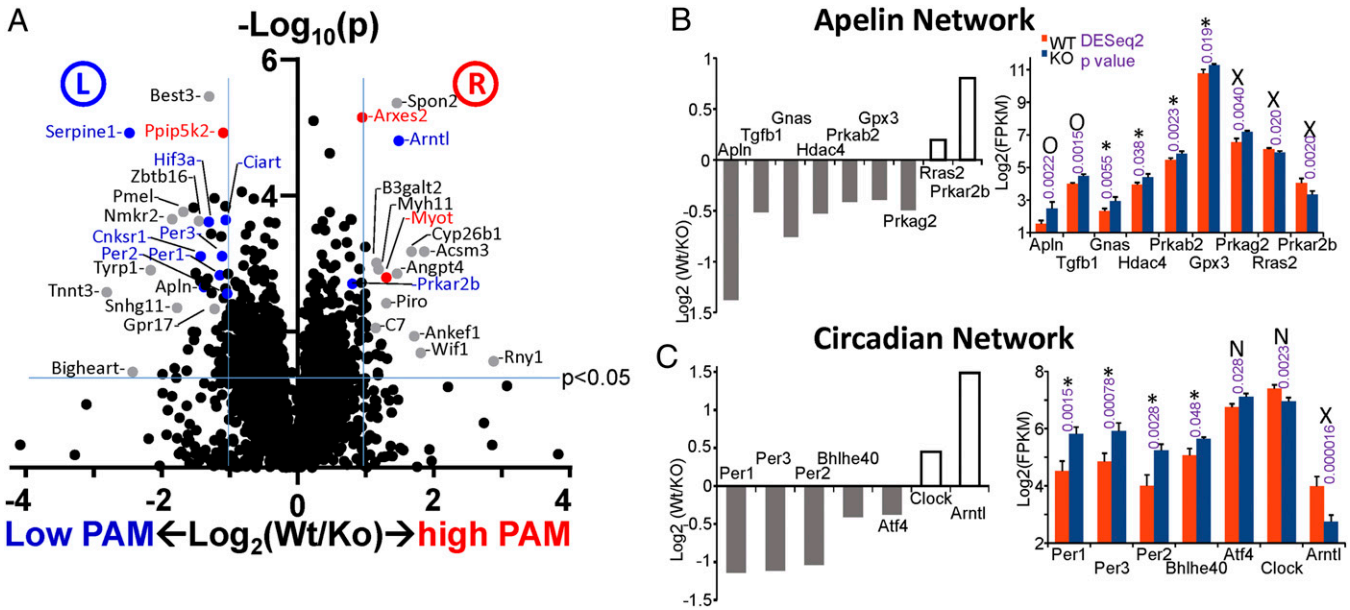

Fig. 8. RNAseq of atrial RNA. (*A*) Volcano plot of all transcripts with FPKM > 1 comparing WT and *Pam*$^{Myh6\text{-}cKO/cKO}$ samples; the horizontal blue line indicates the cutoff for DESeq2 significance ($P < 0.05$), while the vertical blue lines indicate transcripts changed at least 2-fold up or down comparing WT and *Pam*$^{Myh6\text{-}cKO/cKO}$ samples. The *x* axis is $\log_2$ of the ratio (WT/knockout [KO]); the *y* axis is −log10 of the DESeq2 *P* value (up is more significant). Transcripts with blue dots were decreased when PAM was induced in pituitary cells in our previous study (10), while red dots indicate transcripts increased when PAM was induced. Gray dots indicate transcripts expressed at low levels in pituitary cells (FPKM < 3). (*B* and *C*) From IPA, 2 of the most significant networks were centered on the apelin peptide and on circadian rhythms. The *y* axes of the bar graphs in *Left* show $\log_2$ of the WT/KO ratio. The *y* axes of the bar graphs in *Right* show $\log_2$ of the FPKM values for each transcript in WT and KO along with the DESeq2 *P* value. N, no change in pituitary cells; X, opposite response in pituitary cells; 0, not expressed above FPKM = 2 in pituitary cells. *Significant in pituitary cells (10).

proapelin may yield multiple peptides with different biological activities. After experimentally induced pressure overload due to aortic banding, *Apln* knockout mice exhibit severely reduced cardiac contractility (80).

The generation of a PAM-derived COOH-terminal fragment called sfCD, which enters the nucleus (25), led to studies on the effects of PAM on gene expression. We know from our studies in a doxycycline-inducible corticotrope tumor cell line that a 2-d 100-fold increase in PAM expression (up close to the level in the adult atrium) altered the expression of a few hundred genes (10). The altered atrial gene expression observed here could reflect the absence of PAM itself or a compensatory response to the consequences of lacking PAM expression since conception. It is particularly interesting to note the large number of transcripts, which change in response to altered PAM expression in both pituitary cells and atrium. Of the 100 transcripts most altered in the atrium by PAM deletion since conception (quadrants L and R in Fig. 8*A*) (with DESeq2 $P < 0.05$ and more than a 2-fold change), over a third were also responsive to a 48-h increase in PAM expression in pituitary cells (10). A majority of these changes correlated with PAM levels in these 2 very different model systems (*SI Appendix*, Table S3).

One particularly interesting set of transcripts is intimately involved in circadian rhythms (*SI Appendix*, Table S3). Clock and Arntl(Bmal1) (both decreased in atria of $Pam^{Myh6\text{-}cKO/cKO}$ mice) form a dimeric transcription complex that normally stimulates expression of Cryptochrome (Cry) and Period (Per), which then form another heterodimer that negatively feeds back onto Clock and Arntl (81, 82). In the $Pam^{Myh6\text{-}cKO/cKO}$ mice, Per1, Per2, and Per3 transcripts all increased more than 2-fold, and Cry2 rose 50% (Cry1 was much lower and unchanged). Among other circadian transcripts, Ciart(Gm129; Chrono) doubled, and Serpine1(Pai-1) rose 6-fold. Normally, the Clock-Arntl heterodimer is described as the activator, increasing all Per transcripts and Cry; the Per-Cry heterodimer feedback represses Clock-Arntl (81, 82). Bhlhe40 (Dec1) increased significantly, acting to suppress the Clock/Arntl activation of Per and Cry. The pattern of atrial mRNA in $Pam^{Myh6\text{-}cKO/cKO}$ mice (Per-Cry elevated, Clock-Arntl decreased) mimics the latter part of the light–dark cycle; interestingly, the majority of myocardial infarctions occur at the start of the light cycle (83). Strikingly, 7 of 8 circadian transcripts discussed responded to changes in PAM expression in the same manner in the atrium and in corticotrope tumor cells (*SI Appendix*, Table S3).

ACKNOWLEDGMENTS. We thank Dr. Nils Bäck for the broad perspective that he provided as he offered comments on this manuscript and members of the Neuropeptide Laboratory for many helpful discussions. This work was supported by NIH Grants R01DK032948 and R01DK032949, the Janice and Rodney Reynolds Endowment, and the Daniel Schwartzberg Fund.

1. A. Senatore, T. S. Reese, C. L. Smith, Neuropeptidergic integration of behavior in *Trichoplax adhaerens*, an animal without synapses. *J. Exp. Biol.* **220**, 3381–3390 (2017).
2. F. Varoqueaux *et al*., High cell diversity and complex peptidergic signaling underlie placozoan behavior. *Curr. Biol.* **28**, 3495–3501.e2 (2018).
3. M. P. Nusbaum, D. M. Blitz, E. Marder, Functional consequences of neuropeptide and small-molecule co-transmission. *Nat. Rev. Neurosci.* **18**, 389–403 (2017).
4. B. Ramos-Molina, M. G. Martin, I. Lindberg, PCSK1 variants and human obesity. *Prog. Mol. Biol. Transl. Sci.* **140**, 47–74 (2016).
5. L. D. Fricker, Carboxypeptidase E and the identification of novel neuropeptides as potential therapeutic targets. *Adv. Pharmacol.* **82**, 85–102 (2018).
6. X. Liang, T. E. Holy, P. H. Taghert, A series of suppressive signals within the Drosophila circadian neural circuit generates sequential daily outputs. *Neuron* **94**, 1173–1189.e4 (2017).
7. Y. Nakagawa, T. Nishikimi, K. Kuwahara, Atrial and brain natriuretic peptides: Hormones secreted from the heart. *Peptides* **111**, 18–25 (2019).
8. D. Kumar, R. E. Mains, B. A. Eipper, 60 YEARS OF POMC: From POMC and α-MSH to PAM, molecular oxygen, copper, and vitamin C. *J. Mol. Endocrinol.* **56**, T63–T76 (2016).
9. K. Tatemoto, M. Carlquist, V. Mutt, Neuropeptide Y–A novel brain peptide with structural similarities to peptide YY and pancreatic polypeptide. *Nature* **296**, 659–660 (1982).
10. R. E. Mains, C. Blaby-Haas, B. A. Rheaume, B. A. Eipper, Changes in corticotrope gene expression upon increased expression of peptidylglycine α-amidating monooxygenase. *Endocrinology* **159**, 2621–2639 (2018).
11. T. A. Czyzyk *et al*., Deletion of peptide amidation enzymatic activity leads to edema and embryonic lethality in the mouse. *Dev. Biol.* **287**, 301–313 (2005).
12. N. Jiang *et al*., PHM is required for normal developmental transitions and for biosynthesis of secretory peptides in Drosophila. *Dev. Biol.* **226**, 118–136 (2000).
13. D. Kumar *et al*., Microvillar and ciliary defects in zebrafish lacking an actin-binding bioactive peptide amidating enzyme. *Sci. Rep.* **8**, 4547 (2018).
14. D. Bousquet-Moore *et al*., Interactions of peptide amidation and copper: Novel biomarkers and mechanisms of neural dysfunction. *Neurobiol. Dis.* **37**, 130–140 (2010).
15. M. K. H. Schafer, D. A. Stoffers, B. A. Eipper, S. J. Watson, Expression of peptidylglycine alpha-amidating monooxygenase (EC 1.14.17.3) in the rat central nervous system. *J. Neurosci.* **12**, 222–234 (1992).
16. J. A. Gorski *et al*., Cortical excitatory neurons and glia, but not GABAergic neurons, are produced in the Emx1-expressing lineage. *J. Neurosci.* **22**, 6309–6314 (2002).
17. P. Li *et al*., Loss of CLOCK results in dysfunction of brain circuits underlying focal epilepsy. *Neuron* **96**, 387–401.e6 (2017).
18. D. A. Stoffers, C. B. Green, B. A. Eipper, Alternative mRNA splicing generates multiple forms of peptidyl-glycine alpha-amidating monooxygenase in rat atrium. *Proc. Natl. Acad. Sci. U.S.A.* **86**, 735–739 (1989).
19. R. Agah *et al*., Gene recombination in postmitotic cells. Targeted expression of Cre recombinase provokes cardiac-restricted, site-specific rearrangement in adult ventricular muscle in vivo. *J. Clin. Invest.* **100**, 169–179 (1997).
20. J. Palermo, J. Gulick, M. Colbert, J. Fewell, J. Robbins, Transgenic remodeling of the contractile apparatus in the mammalian heart. *Circ. Res.* **78**, 504–509 (1996).
21. K. S. Vishwanatha, N. Bäck, T. T. Lam, R. E. Mains, B. A. Eipper, O-glycosylation of a secretory granule membrane enzyme is essential for its endocytic trafficking. *J. Biol. Chem.* **291**, 9835–9850 (2016).
22. M. B. Miller *et al*., Brain region and isoform-specific phosphorylation alters Kalirin SH2 domain interaction sites and calpain sensitivity. *ACS Chem. Neurosci.* **8**, 1554–1569 (2017).
23. C. C. Glembotski, C. E. Irons, A. B. Sprenkle, C. A. Sei, Studies of ANF processing and secretion using a primary cardiocyte culture model. *Can. J. Physiol. Pharmacol.* **69**, 1525–1536 (1991).
24. P. P. Shields, C. C. Glembotski, The post-translational processing of rat pro-atrial natriuretic factor by primary atrial myocyte cultures. *J. Biol. Chem.* **263**, 8091–8098 (1988).
25. C. Rajagopal, K. L. Stone, V. P. Francone, R. E. Mains, B. A. Eipper, Secretory granule to the nucleus: Role of a multiply phosphorylated intrinsically unstructured domain. *J. Biol. Chem.* **284**, 25723–25734 (2009).
26. I. R. Sarda, M. L. de Bold, A. J. de Bold, Optimization of atrial natriuretic factor radioimmunoassay. *Clin. Biochem.* **22**, 11–15 (1989).
27. S. W. M. John *et al*., Genetic decreases in atrial natriuretic peptide and salt-sensitive hypertension. *Science* **267**, 679–681 (1995).
28. P. Mandela, Y. Yan, T. LaRese, B. A. Eipper, R. E. Mains, Elimination of Kalrn expression in POMC cells reduces anxiety-like behavior and contextual fear learning. *Horm. Behav.* **66**, 430–438 (2014).
29. X. M. Ma, R. E. Mains, B. A. Eipper, Plasticity in hippocampal peptidergic systems induced by repeated electroconvulsive shock. *Neuropsychopharmacology* **27**, 55–71 (2002).
30. X. M. Ma, Y. Wang, F. Ferraro, R. E. Mains, B. A. Eipper, Kalirin-7 is an essential component of both shaft and spine excitatory synapses in hippocampal interneurons. *J. Neurosci.* **28**, 711–724 (2008).
31. X. M. Ma *et al*., Kalirin-7 is required for synaptic structure and function. *J. Neurosci.* **28**, 12368–12382 (2008).
32. D. D. Kiraly *et al*., Behavioral and morphological responses to cocaine require kalirin7. *Biol. Psychiatry* **68**, 249–255 (2010).
33. T. P. LaRese, B. A. Rheaume, R. Abraham, B. A. Eipper, R. E. Mains, Sex-specific gene expression in the mouse nucleus accumbens before and after cocaine exposure. *J. Endocr. Soc.* **3**, 468–487 (2019).
34. D. M. L. Vianna, P. Carrive, Changes in cutaneous and body temperature during and after conditioned fear to context in the rat. *Eur. J. Neurosci.* **21**, 2505–2512 (2005).
35. R. A. Piñol *et al*., Brs3 neurons in the mouse dorsomedial hypothalamus regulate body temperature, energy expenditure, and heart rate, but not food intake. *Nat. Neurosci.* **21**, 1530–1540 (2018).
36. S. E. Whitesall, J. B. Hoff, A. P. Vollmer, L. G. D'Alecy, Comparison of simultaneous measurement of mouse systolic arterial blood pressure by radiotelemetry and tail-cuff methods. *Am. J. Physiol. Heart Circ. Physiol.* **286**, H2408–H2415 (2004).
37. L. G. Melo, M. E. Steinhelper, S. C. Pang, Y. Tse, U. Ackermann, ANP in regulation of arterial pressure and fluid-electrolyte balance: Lessons from genetic mouse models. *Physiol. Genomics* **3**, 45–58 (2000).
38. J. Zacharia, J. R. H. Mauban, H. Raina, S. A. Fisher, W. G. Wier, High vascular tone of mouse femoral arteries in vivo is determined by sympathetic nerve activity via α1A- and α1D-adrenoceptor subtypes. *PLoS One* **8**, e65969 (2013).
39. E. D. Gaier *et al*., In vivo and in vitro analyses of amygdalar function reveal a role for copper. *J. Neurophysiol.* **111**, 1927–1939 (2014).
40. S. L. Robinson, T. E. Thiele, The role of neuropeptide Y (NPY) in alcohol and drug abuse disorders. *Int. Rev. Neurobiol.* **136**, 177–197 (2017).

41. D. A. Perrey, Y. Zhang, Therapeutics development for addiction: Orexin-1 receptor antagonists. *Brain Res.*, 10.1016/j.brainres.2018.08.025 (2018).
42. S. J. Simmons, T. A. Gentile, Cocaine abuse and midbrain circuits: Functional anatomy of hypocretin/orexin transmission and therapeutic prospect. *Brain Res.*, 10.1016/j.brainres.2019.02.026 (2019).
43. M. H. James, S. V. Mahler, D. E. Moorman, G. Aston-Jones, A decade of orexin/hypocretin and addiction: Where are we now? *Curr. Top. Behav. Neurosci.* **33**, 247–281 (2017).
44. C. A. Pedersen, Oxytocin, tolerance, and the dark side of addiction. *Int. Rev. Neurobiol.* **136**, 239–274 (2017).
45. S. M. Tyree, L. de Lecea, Lateral hypothalamic control of the ventral tegmental area: Reward evaluation and the driving of motivated behavior. *Front. Syst. Neurosci.* **11**, 50 (2017).
46. S. B. G. Abbott, C. B. Saper, Median preoptic glutamatergic neurons promote thermoregulatory heat loss and water consumption in mice. *J. Physiol.* **595**, 6569–6583 (2017).
47. J. Siemens, G. B. Kamm, Cellular populations and thermosensing mechanisms of the hypothalamic thermoregulatory center. *Pflugers Arch.* **470**, 809–822 (2018).
48. E. Muth, W. J. Driscoll, A. Smalstig, G. Goping, G. P. Mueller, Proteomic analysis of rat atrial secretory granules: A platform for testable hypotheses. *Biochim. Biophys. Acta* **1699**, 263–275 (2004).
49. P. J. O'Donnell, W. J. Driscoll, N. Back, E. Muth, G. P. Mueller, Peptidylglycine-α-amidating monooxygenase and pro-atrial natriuretic peptide constitute the major membrane-associated proteins of rat atrial secretory granules. *J. Mol. Cell. Cardiol.* **35**, 915–922 (2003).
50. V. Labrador, C. Brun, S. König, A. Roatti, A. J. Baertschi, Peptidyl-glycine alpha-amidating monooxygenase targeting and shaping of atrial secretory vesicles: Inhibition by mutated N-terminal ProANP and PBA. *Circ. Res.* **95**, e98–e109 (2004).
51. F. Wu, W. Yan, J. Pan, J. Morser, Q. Wu, Processing of pro-atrial natriuretic peptide by corin in cardiac myocytes. *J. Biol. Chem.* **277**, 16900–16905 (2002).
52. S. Fu, P. Ping, F. Wang, L. Luo, Synthesis, secretion, function, metabolism and application of natriuretic peptides in heart failure. *J. Biol. Eng.* **12**, 2 (2018).
53. M. F. McGrath, M. L. K. de Bold, A. J. de Bold, The endocrine function of the heart. *Trends Endocrinol. Metab.* **16**, 469–477 (2005).
54. K. Sato, T. Numata, T. Saito, Y. Ueta, Y. Okada, V_2 receptor-mediated autocrine role of somatodendritic release of AVP in rat vasopressin neurons under hypo-osmotic conditions. *Sci. Signal.* **4**, ra5 (2011).
55. K. N. Pandey, Molecular and genetic aspects of guanylyl cyclase natriuretic peptide receptor-A in regulation of blood pressure and renal function. *Physiol. Genomics* **50**, 913–928 (2018).
56. A. J. Miller, A. C. Arnold, The renin-angiotensin system in cardiovascular autonomic control: Recent developments and clinical implications. *Clin. Autonom. Res.* **29**, 231–243 (2019).
57. P. F. O'Tierney, M. Y. Tse, S. C. Pang, Elevated renal norepinephrine in proANP gene-disrupted mice is associated with increased tyrosine hydroxylase expression in sympathetic ganglia. *Regul. Pept.* **143**, 90–96 (2007).
58. S. Zhang, F. Zhang, H. Sun, Y. Zhou, Y. Han, Enhanced sympathetic activity and cardiac sympathetic afferent reflex in rats with heart failure induced by adriamycin. *J. Biomed. Res.* **26**, 425–431 (2012).
59. H. Antushevich, M. Wójcik, Review: Apelin in disease. *Clin. Chim. Acta* **483**, 241–248 (2018).
60. A. Nakashima *et al.*, Dec1 and CLOCK regulate Na^+/K^+-ATPase β1 subunit expression and blood pressure. *Hypertension* **72**, 746–754 (2018).
61. H. J. Pi *et al.*, Cortical interneurons that specialize in disinhibitory control. *Nature* **503**, 521–524 (2013).
62. Q. Wei *et al.*, Uneven balance of power between hypothalamic peptidergic neurons in the control of feeding. *Proc. Natl. Acad. Sci. U.S.A.* **115**, E9489–E9498 (2018).
63. F. Sotres-Bayon, D. E. Bush, J. E. LeDoux, Acquisition of fear extinction requires activation of NR2B-containing NMDA receptors in the lateral amygdala. *Neuropsychopharmacology* **32**, 1929–1940 (2007).
64. C. M. Fraser, M. J. Cooke, A. Fisher, I. D. Thompson, T. W. Stone, Interactions between ifenprodil and dizocilpine on mouse behaviour in models of anxiety and working memory. *Eur. Neuropsychopharmacol.* **6**, 311–316 (1996).
65. P. W. Kalivas, N. D. Volkow, New medications for drug addiction hiding in glutamatergic neuroplasticity. *Mol. Psychiatry* **16**, 974–986 (2011).
66. C. D. Gipson, Y. M. Kupchik, P. W. Kalivas, Rapid, transient synaptic plasticity in addiction. *Neuropharmacology* **76**, 276–286 (2014).
67. D. M. Walker *et al.*, Cocaine self-administration alters transcriptome-wide responses in the brain's reward circuitry. *Biol. Psychiatry* **84**, 867–880 (2018).
68. A. Ströhle, C. Feller, C. J. Strasburger, A. Heinz, F. Dimeo, Anxiety modulation by the heart? Aerobic exercise and atrial natriuretic peptide. *Psychoneuroendocrinology* **31**, 1127–1130 (2006).
69. C. Herrmann-Lingen *et al.*, High plasma levels of N-terminal pro-atrial natriuretic peptide associated with low anxiety in severe heart failure. *Psychosom. Med.* **65**, 517–522 (2003).
70. Z. D. Zhao *et al.*, A hypothalamic circuit that controls body temperature. *Proc. Natl. Acad. Sci. U.S.A.* **114**, 2042–2047 (2017).
71. A. Morelli *et al.*, Metabolic syndrome induces inflammation and impairs gonadotropin-releasing hormone neurons in the preoptic area of the hypothalamus in rabbits. *Mol. Cell. Endocrinol.* **382**, 107–119 (2014).
72. D. Xi *et al.*, Ablation of oxytocin neurons causes a deficit in cold stress response. *J. Endocr. Soc.* **1**, 1041–1055 (2017).
73. U. Ernsberger, M. Kramer, K. Tsarovina, T. Deller, H. Rohrer, Coordinate expression of pan-neuronal and functional signature genes in sympathetic neurons. *Cell Tissue Res.* **370**, 227–241 (2017).
74. J. C. Y. Chan *et al.*, Hypertension in mice lacking the proatrial natriuretic peptide convertase corin. *Proc. Natl. Acad. Sci. U.S.A.* **102**, 785–790 (2005).
75. T. W. Kurtz, S. E. DiCarlo, M. Pravenec, R. C. Morris, Jr, An appraisal of methods recently recommended for testing salt sensitivity of blood pressure. *J. Am. Heart Assoc.* **6**, e005653 (2017).
76. A. J. de Bold *et al.*, A decade of atrial natriuretic factor research. *Can. J. Physiol. Pharmacol.* **69**, 1480–1485 (1991).
77. K. Inoue, Y. Takei, Molecular evolution of the natriuretic peptide system as revealed by comparative genomics. *Comp. Biochem. Physiol. Part D Genomics Proteomics* **1**, 69–76 (2006).
78. H. Ogawa, Y. Qiu, C. M. Ogata, K. S. Misono, Crystal structure of hormone-bound atrial natriuretic peptide receptor extracellular domain: Rotation mechanism for transmembrane signal transduction. *J. Biol. Chem.* **279**, 28625–28631 (2004).
79. H. Ogawa *et al.*, Structure of the atrial natriuretic peptide receptor extracellular domain in the unbound and hormone-bound states by single-particle electron microscopy. *FEBS J.* **276**, 1347–1355 (2009).
80. K. Kuba *et al.*, Impaired heart contractility in Apelin gene-deficient mice associated with aging and pressure overload. *Circ. Res.* **101**, e32–e42 (2007). Erratum in: *Circ. Res.* **102**, e36 (2008).
81. K. Singh, N. K. Jha, A. Thakur, Spatiotemporal chromatin dynamics–A telltale of circadian epigenetic gene regulation. *Life Sci.* **221**, 377–391 (2019).
82. X. Zhao *et al.*, Nuclear receptors rock around the clock. *EMBO Rep.* **15**, 518–528 (2014).
83. K. Maemura, N. Takeda, R. Nagai, Circadian rhythms in the CNS and peripheral clock disorders: Role of the biological clock in cardiovascular diseases. *J. Pharmacol. Sci.* **103**, 134–138 (2007).